ELSEVIER
SAUNDERS

Neurosurg Clin N Am 16 (2005) 101–114

NEUROSURGERY
CLINICS
OF NORTH AMERICA

Proton magnetic resonance spectroscopic imaging in brain tumor diagnosis

Stephen Gruber, PhD[a,b], Andreas Stadlbauer, PhD[a,b], Vladimir Mlynarik, PhD[a], Brigitte Gatterbauer, MD[c], Karl Roessler, MD[c], Ewald Moser, PhD[a,b,d,*]

[a]*Magnetic Resonance Centre of Excellence, Medical University of Vienna, Lazarettgasse 14, A-1090 Vienna, Austria*
[b]*Department of Medical Physics, Medical University of Vienna, Kompetenzzentrum Hochfeld-MR (MR-Holzhaus), A-1090 Vienna, Lazarettgasse 14, Austria*
[c]*Department of Neurosurgery, Medical University of Vienna, Kompetenzzentrum Hochfeld-MR (MR-Holzhaus), A-1090 Vienna, Lazarettgasse 14, Austria*
[d]*Department of Radiodiagnostics, Medical University of Vienna, Waehringer Guertel 18–20, A-1090 Vienna, Austria*

Over the last 15 years, single-voxel and multivoxel proton magnetic resonance spectroscopy (^{1}H-MRS) and ^{1}H-magnetic resonance spectroscopic imaging (MRSI) have become useful tools in supporting the understanding and diagnosis of a number of clinical pathologic findings, particularly brain tumors. Several excellent reviews document this progress [1–6]. Primary brain tumors are recognized and characterized not only via the lesion size but also via the pathologic metabolism, although this is quite heterogeneous [7,8]. This limits the use of established (invasive) diagnostic approaches, namely, conventional contrast-enhanced MRI (CE-MRI) at 1.5 T, with a diagnostic accuracy of 30% to 90% depending on tumor type [9,10], and the "gold standard" of brain biopsy. Brain biopsy is a heavily invasive technique with minor morbidity in up to 3.3% of cases, major morbidity in up to 3.6% of cases, a hemorrhage rate up to 8% of cases, and mortality in up to 1.7% of cases, as assessed over a large number of studies [11–15]. Diagnostic accuracy is 91% (low-grade astrocytoma), 83% (anaplastic astrocytoma), and 88% (glioblastoma multiforme). The histologic grade of malignancy, however, is predictable, with an accuracy of only 57% to 61% [16]. Differentiation between brain abscess and cystic or necrotic brain tumor using CT or MRI has not been particularly successful to date [17,18], although Arnold et al [19] have shown similar performance to brain biopsy. Early identification and differentiation of brain abscesses and malignant brain tumors should be followed by the selection of appropriate treatment strategies to improve outcome or the survival rate, particularly in heterogeneous tumors, whether of low or high grade.

What is Magnetic Resonance Spectroscopy?

MRS is based on the magnetic interaction between tiny magnetic moments (spins) of atomic nuclei of the body and an external (static) magnetic field of the strength B_0 (in tesla), produced by the magnetic resonance scanner. This interaction is modulated by electrons surrounding atomic nuclei, resulting in molecule-specific absorption lines in so-called "nuclear magnetic resonance (NMR) spectra." The original term "nuclear magnetic

This study was financially supported by the Austrian Science Fund (FWF P14715-PSY to E. Moser) and the German Science Foundation (DFG Ga 638/2-1 to O. Ganslandt).

S. Gruber and A. Stadlbauer contributed equally to this work.

* Corresponding author.
E-mail address: ewald.moser@meduniwien.ac.at (E. Moser).

doi:10.1016/j.nec.2004.07.004

resonance" already contains all essential aspects: (1) the atomic nucleus with a detectable spin, (2) the magnetic interaction between spins and external (static and radiofrequency) magnetic fields, and (3) the resonance condition that has to be fulfilled between the frequency of the external magnetic field and the frequency of the spin precession. This magnetic interaction results in a time-dependent (high-frequency) magnetic response of the spin system, which is called free induction decay (FID). The FID contains various frequency components that can be identified via the Fourier transform (FT), resulting in a characteristic pattern or spectrum. Using additional magnetic fields for localization, characteristic spectra may be observed from defined regions in the body. The appearance of these spectra depends on general conditions, that is, which NMR-sensitive nuclei (eg, hydrogen [protons (^{1}H)], carbon [^{13}C], phosphorus [^{31}P]) are to be studied, instrumental (eg, field strength [B_0]) and methodologic parameters (eg, spatial localization or water suppression techniques) and, of course, the biochemical composition and architecture of the tissue studied. Examples may be found in several excellent textbooks on clinical MRS [20,21].

Currently, ^{1}H-MRS is the most frequently used methodology in tumor diagnosis [22]. Because MRS is basically a low-sensitivity method, only metabolites above approximately 0.5 mmol in brain tissue may be detected. Thus, only spectral lines of *N*-acetylaspartate (NAA, at approximately 2.0 ppm), choline (Cho)-containing compounds at approximately 3.2 ppm, total creatine (Cr) and phosphocreatine at approximately 3.0 and 3.9 ppm, myoinositol (mINS, two lines at approximately 3.6 ppm), a mixture of glutamine and glutamate (Glx, overlapping multiplets at approximately 2.0–2.5 ppm and 3.75 ppm, respectively), lactate (Lac, doublet at approximately 1.3 ppm), and lipids (Lip, broad lines at 0.9 and 1.3 ppm) [23,24] may be observed if not always quantified. An example of a single-voxel short–echo time (TE) proton spectrum of human brain tissue is given in Fig. 1, including assignments of spectral lines. For tumor diagnosis, spectral lines of NAA and Cho are of primary importance. NAA is seen as a neuronal marker, which may be reduced if neurons are being replaced by tumor cells, whereas Cho is thought to reflect cell membrane, myelin, and Lip turnover, leading to increased MRS-visible Cho resonances. The lines of Cr are reduced

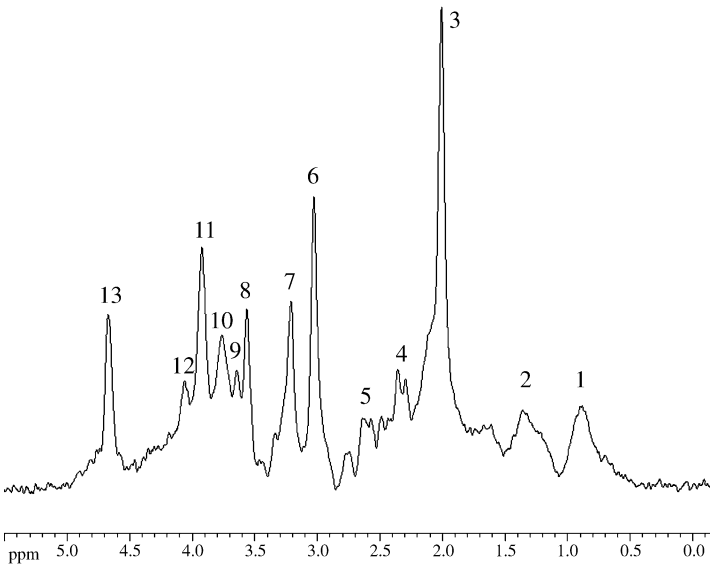

Fig. 1. Single-voxel spectrum from occipital gray matter of a healthy volunteer, obtained at 3 T using a 10-cm surface coil (echo time [TE]/repetition time [TR] = 9/2500 milliseconds, voxel size = 16 cm^3, 384 averages). The spectral lines are assigned as follows: 1, 2 = macromolecules/lipids; 3 = *N*-acetylaspartate (NAA; + N-acetylaspertylglutamate [NAAG] + glucose [Glu] + glutamine [Gln]); 4 = Glu; 5 = NAA; 6 = total creatine (Cr; Cr + phosphocreatine [PCr]); 7 = choline [Cho] (+ myoinositol [mINS]); 8, 9 = mINS; 10 = Glu + Gln; 11 = total Cr; 12 = mINS; 13 = residual water. Note that the excellent signal-to-noise ratio (SNR) is a result of the large voxel size and number of averages, resulting in a measurement time of 16 minutes for a single spectrum as well as the use of a surface coil and very short TE.

in necrotic areas, Lip increases in some high-grade tumors, and Lac is not visible in normal brain but transiently increases in pathologic (anaerobic) metabolism. Automated spectrum-fitting programs (eg, LCModel [25] or VARPRO [26]) and pattern recognition techniques (if a sufficient number of data sets are available [27–29]) may be used to support a diagnosis, because the interpretation of spectra still requires some experience as well as some technical know-how to identify artifacts and to assess the quality of (pathologic) spectra.

Application of proton magnetic resonance spectroscopy and magnetic resonance spectroscopic imaging in brain tumor diagnosis

Several studies and reviews suggest that in vivo ^{1}H-MRS might significantly contribute to brain tumor characterization and staging. Most importantly, ^{1}H-MRS is a noninvasive approach that allows monitoring of metabolic changes as a result of tumor-induced pathologic conditions, with the potential to diagnose the presence of tumors, to differentiate tumors from other pathologic processes of similar appearance (eg, brain abscesses), and to characterize the stage of tumor development. Although the brain metabolites detectable via ^{1}H-MRS in vivo are not tumor specific, distinct metabolic patterns [24] and changes have been reported in ^{1}H-MRS applications in human brain tumors (for recent reviews, see the articles by Burtscher and Holtas [5], Smith et al [22], and Howe and Opstad [6], and Kwock et al [30]).

Most ^{1}H-MRS brain tumor studies to date have been performed at 1.5 T using localized single-voxel spectroscopy or spectroscopic imaging with relatively low spatial resolution (approximately 1–8 cm^3) compared with conventional MRI, with resolutions of approximately 1 mm^3. This was a common obstacle in early tumor studies [31]. Ricci et al [32] pointed out that the positioning of single-voxel spectra influences the accuracy of findings in tumor ^{1}H-MRS. They reported that from voxels positioned centrally within the lesion, the ^{1}H-MRS findings reflected histologic outcome in only two of nine lesions, whereas including the enhancing edge of the lesions allowed correct classification of seven of eight lesions. High spatial resolution may increase specificity, although at the cost of reduced sensitivity, and thus plays an important role in the clinical application of ^{1}H-MRS in human brain tumor diagnosis and therapy monitoring.

Localized spectroscopy measurements and quantification are straightforward and were approved by the US Food and Drug Administration (FDA) in 1995. One or more cubic voxels are measured within one session, using relatively large (3–8 cm^3) volumes. Data can be absolutely quantified using a number of commercially available software tools (eg, LCModel) [25,33]. The relatively large voxel size in single-voxel spectroscopy prevents accurate matching of different anatomic or pathologic structures, however, reducing diagnostic specificity.

In contrast, two-dimensional (2D) or three-dimensional (3D) MRSI enables the collection of spectra from several hundreds or thousand of voxels within one session, although only some may be of diagnostic relevance. Because one large area is measured at one time/session, exact positioning is not critical. Depending on the technique used for spatial encoding, the actual position of the measured voxels can be shifted after data collection using techniques like zero filling or (the mathematically equivalent) voxel shifting [34,35]. Of special interest is the computation of metabolic maps (eg, by integrating the area under a given peak in the spectrum for each voxel) to monitor the spatial distribution of metabolic changes. A number of methods have been proposed for absolute quantification of MRSI data. McLean et al [36] developed an automatic routine overlay for large 2D MRSI data sets to obtain quantitative metabolic maps using the LCModel. At 1.5 T, 0.5 cm^3 represents the approximate resolution limit within tolerable measurement times of 10 to 15 minutes for 2D chemical shift imaging (CSI) or 50 minutes for 3D MRSI with four slices using head volume coils [37].

Based on matured hardware and software as well as increasing clinical experience, the following clinical applications or studies using in vivo ^{1}H-MRS, as summarized by Howe and Opstad [6], are currently underway: (1) noninvasive diagnosis of a mass or lesion in the brain, (2) tumor grading, (3) noninvasive follow-up of therapeutic response and progression, (4) therapeutic planning, and (5) prognostic information on patient survival.

We proceed to an example of contemporary clinical ^{1}H-MRS, describing a typical measurement session and showing clinical data. These were obtained from a routine clinical 1.5-T scanner installed in a surgical theater using a 2D CSI localization technique with the highest possible spatial resolution and software developed in-house to quantify and visualize metabolic changes in and around tumors and to correlate these MRS-based

results with the neuronavigation system. The final section describes cutting-edge achievements in spectroscopic imaging at 3 T. We conclude with an outlook of the prospects for faster data collection, which should increase patient comfort, and even higher field strengths in MRS of the brain.

Description of noninvasive 1.5-T MRI/magnetic resonance spectroscopic imaging sessions

Patients, all with untreated supratentorial gliomas (World Health Organization [WHO] grade II–IV), and matched controls are examined on a 1.5-T clinical whole-body scanner (MAGNETOM Sonata; Siemens Medical, Erlangen, Germany) equipped with the standard head coil. Measurements, data processing, and integration into frameless stereotaxy are performed at the Department of Neurosurgery, University of Erlangen-Nuremberg, Erlangen, Germany.

2D ^{1}H-MRSI experiments are performed in separate sessions after routine MRI for initial lesion diagnosis. Tumor MRI includes (1) an axial turbo spin echo (TSE) sequence (T_2-weighted, 5-mm slices, repetition time [TR]/TE = 4000/98 milliseconds), (2) an axial fluid-attenuated inversion recovery (FLAIR) sequence (5-mm slices, TR/TE = 10,000/103 milliseconds), and (3) pre- and postgadolinium, contrast-enhanced, coronal gradient echo sequences (T_1-weighted, 5-mm slices, TR/TE = 430/12 and 525/17 milliseconds, respectively). In a subsequent MRS session, two localization scans and an axial spin echo (SE) sequence (T_1-weighted) are acquired for MRSI excitation volume location. The T_1-weighted SE sequence is used for matching spectroscopic images to an anatomic 3D MRI set [38]. Typical parameters are TR/TE of 500/15 milliseconds, 256 × 256 matrix size, 16-cm × 16-cm field of view (FOV), 20 slices with no gap, and a slice thickness of 2 mm. The ^{1}H-MRSI slab with point-resolved spectroscopy (PRESS) [39] volume preselection is aligned parallel to the axial localizer slices. Water suppression is achieved using three chemical shift selective (CHESS) [40] pulses before the PRESS excitation. The MRSI parameters are TR/TE of 1600/135 milliseconds, 24 × 24 circular phase-encoding scheme across a 16-cm × 16-cm FOV, 10-mm slice thickness, 50% Hamming filter and two averages, 1000-Hz spectral width, and 1024 complex points of acquisition size. The total spectroscopic data acquisition time is less than 13 minutes, whereas the routine MRI session, including contrast agent application, takes approximately 40 minutes. The nominal voxel size in 2D MRSI is 0.67 cm^3 × 0.67 cm^3 × 1.0 cm^3 (approximately 0.45-cm^3 resolution). Taking into account the effect of the applied k-space filter (50% Hamming filter) [41] on the full-width-at-half-maximum and after zero filling to a 32 × 32 matrix size, the volume of the measured voxels is 0.52 cm^3. The PRESS excitation volume is positioned to cover the whole or at least the bulk of the tumor and as much apparently normal brain tissue as possible.

In a single session 1 day before surgery, a 3D anatomic magnetization–prepared rapid acquisition gradient echo (MPRAGE) sequence is performed with the following parameters: TR/TE of 2020/4.38 milliseconds, 25-cm × 25-cm FOV, 1 mm isotropic, and 160 slices. For registration in a frameless stereotactic system (VectorVisionSky; BrainLab, Heimstetten, Germany) six to eight adhesive skin fiducials are positioned in a scattered pattern on the head surface before imaging. Thus, all MRI and MRSI data may be converted into the same frame of reference with a typical accuracy of 1 mm^3 isotropically.

Data processing

Zero filling to a 32 × 32 matrix size and 2D spatial FT is performed with the manufacturer's data processing software (syngo MR 2002A; Siemens Medical). MRSI raw data sets without any header information are processed with the freely available LINUX-based reconstruction program, CSX, obtained from PB Barker (Baltimore, Maryland). Spectroscopic imaging data are exponentially filtered with a line-broadening factor of 3 Hz, zero filled to 2048 data points, and undergo a FT with respect to the spectral dimension. To remove the residual water peak, we use a high-pass convolution filter (50-Hz stop band) [42]. Magnitude spectra are calculated, the position of NAA is set to 2.02 ppm, and a susceptibility correction is applied. The peak areas for Cho, Cr, and NAA are calculated by integration over the frequency range of 3.34 to 3.14 ppm, 3.14 to 2.94 ppm, and 2.22 to 1.82 ppm, respectively (see Fig. 1). Smooth linear interpolation to a 256 × 256 matrix results in the metabolic maps. Cho and NAA images (Fig. 2) are used to calculate a map of Cho/NAA ratios. Tumor borders are automatically segmented in this Cho/NAA image based on

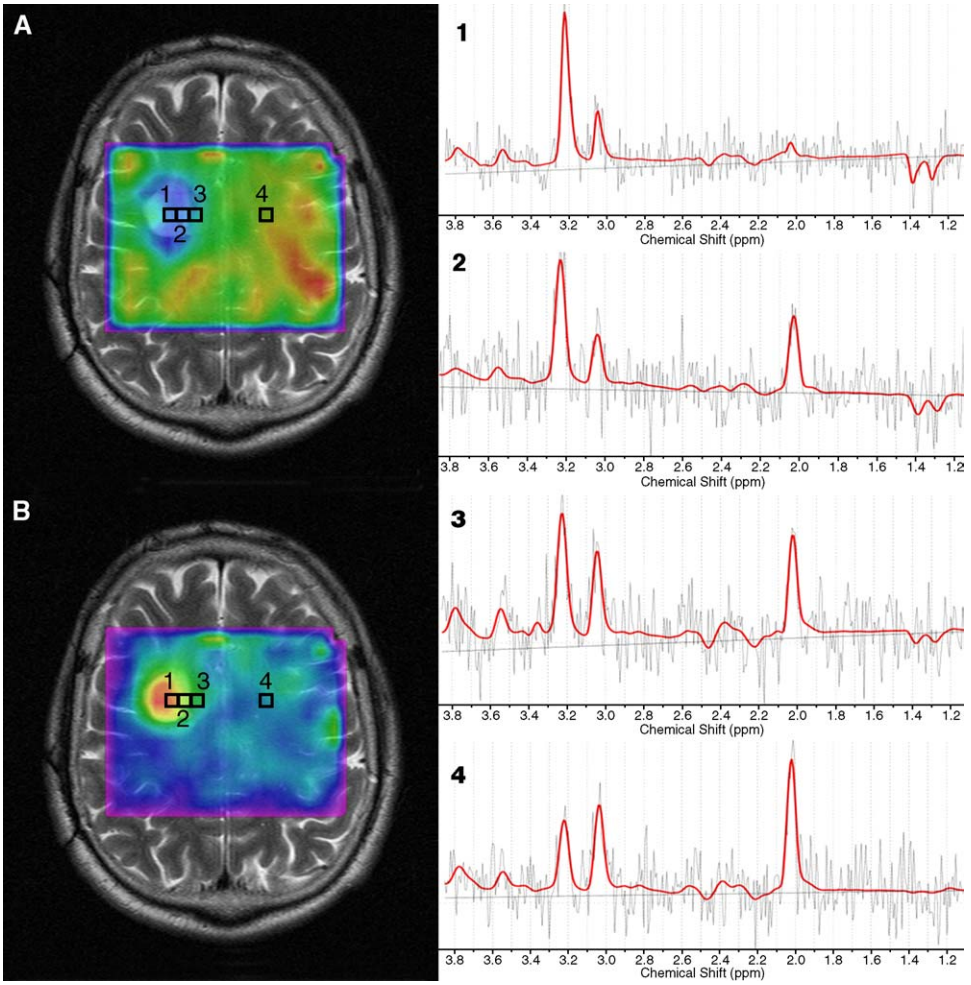

Fig 2. Anatomic images (T2-weighted) overlaid with metabolic maps of a patient with an oligoastrocytoma, World Health Organization grade III. *N*-acetylaspartate map (*A*); choline map (*B*); and spectra of (1) the tumor center, (2) the intermediate zone, (3) the tumor border and (4) contralateral normal brain according to the marked positions in A and B.

the assumption of Gaussian distribution of the Cho/NAA values for normal brain [43].

Coregistration of metabolic and anatomic MRI

Because of the choice of the same FOV and precise alignment of the T_1-weighted SE protocol and the MRSI experiment, direct coregistration of the data of the MRSI slab (10-mm thick) with five slices (each 2-mm thick, no gap) of the anatomic MRI can be achieved [38]. A combined data set consisting of MRI and MRSI data, a so-called "MRI/MRSI hybrid data set," is created and matched exactly to a 3D data set for use with frameless stereotaxy (Fig. 3).

Clinical results at 1.5 T

High-resolution MRSI data of good quality have been obtained from all patients examined. MRSI data analysis, including the calculation of metabolic maps and segmentation as well as the integration of these MRSI results in functional neuronavigation, was successfully performed in most cases. The precision and accuracy of the method have been validated by inspection of the congruency of structural details between the anatomic slices in the hybrid data set and the 3D MPRAGE data set. The total time for performing this procedure was about 1 hour 20 minutes for conventional MRI (SE sequence) and MRSI data acquisition, 30 minutes for MRSI data analysis,

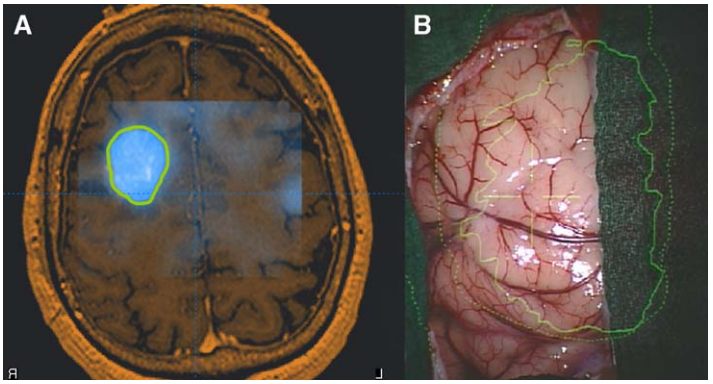

Fig. 3. Image fusion of metabolic maps (MRI/magnetic resonance spectroscopic imaging [MRSI] hybrid data set) and a three-dimensional (3D) MRI data set (same patient as presented in Fig. 2). (*A*) The result is a 3D MRI scan consisting of anatomic (in amber) and metabolic (biochemical, in blue) information for surgical planning. Regions of interest (tumor border) as drawn by the neurosurgeon on the basis of the spectroscopic information are outlined in green. (*B*) Proton (^{1}H)-MRSI–guided frameless stereotaxy: view through the navigation microscope. The maximum and actual tumor borders are outlined in green as dotted and solid lines, respectively.

and 10 minutes for obtaining the MRI/MRSI hybrid data set.

Illustrative case at 1.5 T

A 38-year-old male patient was operated on for the first time for a right frontal tumor in 1999 after a generalized seizure. Histologic examination revealed an oligoastrocytoma (WHO grade II). Two years later, he had new focal seizures and tumor recurrence was seen on MRI scans. We performed surgery with frameless stereotaxy and preoperative functional MRI (fMRI) localization of the motor cortex. During surgery, phase reversal was in complete agreement with the fMRI results and showed the tumor to be one gyrus anterior to the motor cortex. Simultaneously, metabolic maps from ^{1}H-MRSI were integrated into the neuronavigation system (see Fig. 3B) and multiple biopsies were obtained from the tumor borders according to the biochemical information obtained from ^{1}H-MRSI. Intraoperative MRI showed complete tumor removal. The new histopathologic diagnosis documented transformation into an anaplastic oligoastrocytoma (WHO grade III) supported by the ^{1}H-MRSI results [44].

Discussion of clinical results at 1.5 T

^{1}H-MRSI has been used extensively for the evaluation of brain tumors. The major indications for brain tumor spectroscopy have been differential diagnosis, delineation for treatment planning in radiation therapy, stereotactic brain biopsy, and response to treatment. The problem of representation of metabolic changes in brain tumors has been solved using a number of approaches [45–49]. Images of different metabolite ratios (Cho/NAA, Cho/Cr, and Cr/NAA) were used by Li et al [50] for evaluating and characterizing gliomas. De Edelenyi et al [51] showed six major spectral peaks (Cho, Cr, NAA, alanine, Lac or Lip, and Lip) and information contained in T2-weighted MRI in a profile, so-called "nosologic images," and used them for characterization of brain tumors. Fulham et al [46] and McKnight et al [52] showed that images of Cho and NAA are most suitable for tumor spectroscopy. The signal differences between normal brain and tumor are sufficient to show the position of the tumor but not for delineation of the border zone. Also, partial volume effects of cerebrospinal fluid in sulci and ventricles modulate the level of these metabolites in normal brain tissue. This may cause metabolic variations in normal brain regions not related to pathologic changes. In a recent publication, McKnight et al [52] showed that the use of the relative levels of Cho to NAA is also suitable for delineation of the tumor border. They assumed that the relation between Cho and NAA in normal brain could be modeled as a linear function and used this to select voxels as internal controls for quantifying the probability of abnormality at each voxel location in patients with gliomas. In further studies of this group [53,54], they achieved segmentation of brain tumors using this method and the definition of

abnormality index contours. These contours were overlaid on anatomic images or on maps of Cho/NAA and used for target delineation in radiation therapy treatment planning [55].

In addition, a number of recent papers described the integration of functional information (eg, magnetoencephalography [MEG] [56–58] and fMRI [59–61]) into frameless stereotaxy (for a review, see the article by Nimsky et al in this supplement). This implementation of functional imaging and navigation, so-called "functional neuronavigation," covers anatomic and functional data and allows the fast identification of eloquent brain areas. Only a few studies have used MRSI to support biopsy target delineation [62–66] or radiation therapy treatment planning [53,55,60]. None of the cited studies integrated MRSI data in a neuronavigation system and performed intraoperative visualization of MRSI data. Preul et al [67] achieved integration of MRSI data (metabolic maps of Cho) of two patients into an image-guided frameless stereotactic system by computing a transformation between the MRSI space and the global MRI space using the targeting volume acquired immediately before MRSI acquisition. Through this approach, they overcame the fact that MRSI lacks detailed structural information. Our strategy for merging MRSI data to a global 3D MRI data set was the full and accurate integration of metabolic images with coregistered anatomic images (MRI/MRSI hybrid data set), resulting in a data set consisting of anatomic and biochemical information [38,43].

Neuronavigation and anatomic image fusion during neurosurgical procedures for appropriate diagnosis and grading of gliomas have also been established at the Vienna Neurosurgical Clinic for a number of years [68–70]. To promote image fusion with functional and metabolic data sets for presurgical, intraoperative, and postoperative treatment planning, we founded an interdisciplinary scientific study group in 2003 ("NEURONET," Vienna Medical University, Neurosurgical Clinic, together with the Departments of Radiodiagnostics, Medical Physics, Nuclear Medicine, and Neurology; the Clinical Institute of Neurology; and the Institute for Biomedical Engineering and Physics). Direct integration of metabolic positron emission tomography (PET) data and 3-T fMRI data for biopsy planning and preservation of functional brain areas was successfully used in a number of patients. The integration of 3-T MRSI data into the intraoperative neuronavigation setting is currently in progress.

Recent developments in three-dimensional spectroscopic imaging at 3 T

Currently, single-voxel MRS and 2D CSI techniques at 1.5 T are routinely used in clinical metabolic brain mapping. Constant technical and methodologic developments made 3 T research systems available during the early 1990s, growing into almost matured clinical systems by 2002. In combination with stronger and faster gradients, 3 T scanners enable the use of more advanced 3D MRSI techniques with clear advantages over standard 1.5-T systems [33,71,72]. Based on these developments, heterogeneous brain tumors may be diagnosed more reliably by reducing partial volume effects (ie, increasing specificity) without excessive loss of sensitivity (ie, signal-to-noise ratio [SNR] critical for quantification).

With the more common availability of high-field scanners (≥3 T), a significant gain in SNR could be obtained in 3D MRSI [71,72]. Additionally, it has been shown that because of an increased homogeneity in smaller voxels, a sufficient SNR can be achieved using a nominal resolution less than 0.5 cm^3, allowing anatomically or pathologically matched "supravoxels" anatomy-matched voxels (AMVs) to be generated after the measurement [73]. High spatial resolution has the potential to increase the specificity of the measured data using AMVs, because partial volume effects are minimized and retrospective voxel averaging (AMV) preserves sensitivity.

To stimulate future applications, we describe recent developments in 3D MRSI at 3 T using very short (11 milliseconds) or long (135 milliseconds) TE protocols to improve tumor diagnosis and grading by ^{1}H-MRSI. Potential benefits of high-resolution 2D or 3D MRSI for clinical applications on human brain tumors and future methodologic improvements are discussed.

Three-dimensional magnetic resonance spectroscopic imaging at 3 T

Healthy volunteers and tumor patients are scanned in single sessions on a 3-T Medspec S300 (Bruker Biospin, Ettlingen, Germany) using the standard birdcage head coil supplied by the manufacturer. Measurements and data processing are performed at the Magnetic Resonance Centre of Excellence, Medical University of Vienna, Vienna, Austria.

A 3D (single-dimension Hadamard spectroscopic imaging [HSI])/2D CSI ^{1}H-MRSI sequence is used [73]. Eight-centimeter left-to-right (LR) by

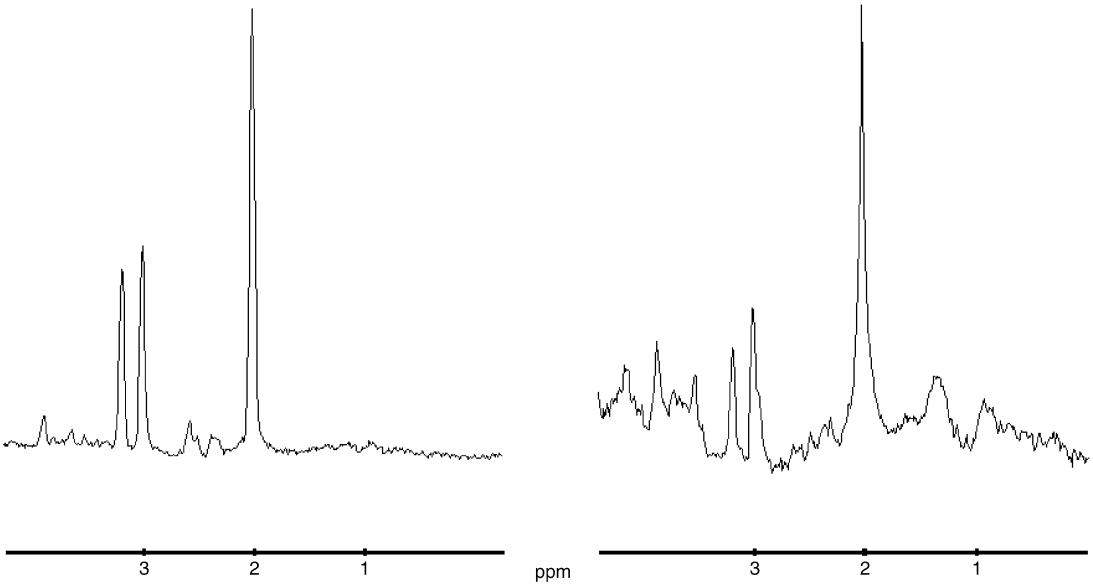

Fig. 4. Anatomy matched voxels spectra of white brain matter (caudal to the ventricles) from two 26-year-old healthy female subjects. (*Left*) One hundred ninety-two zero-filled voxels summed up to 36 cm^3 acquired with point-resolved magnetic resonance spectroscopic imaging (MRSI) (echo time [TE] = 135 milliseconds). (*Right*) One hundred sixty-five zero-filled voxels measured with stimulated echo MRSI (TE = 11 milliseconds). The nominal resolution of both experiments was 0.33 cm^3. Note the different choline/creatine ratios of the short and long TE experiments. Spectra are shown in magnitude mode.

10-cm anterior-posterior (AP) by 3-cm inferior-superior (IS) volumes of interest (VOIs) are excited using the PRESS or stimulated echo (STEAM) localization method with a TE of 135 or 11 milliseconds, respectively, and a TR of 1600 milliseconds. The 16 cm × 16 cm FOV in the LR-AP direction is encoded into a 16 × 16 or 24 × 24 matrix using phase encoding. A total of 1024 complex points are sampled, and a spectral bandwidth of 2500 Hz is used, resulting in an acquisition time of 412 milliseconds. The total measurement time for each session is approximately 27 minutes (patients: nominal resolution of 0.75 cm^3) or 1 hour (healthy volunteers: nominal resolution of 0.33 cm^3). For localization purposes, high-resolution, multislice, rapid acquisition, relaxation-enhanced imaging (RARE, TE/TR = 80/3180 milliseconds) in the axial orientation (512 × 512 matrix size) is performed. Before each experiment, the B_0 field is shimmed in the selected VOI using a fast, automatic stammering technique by mapping along projections pro-

Fig. 5. Anatomic MRI of a brain tumor (*center*) overlaid with the chemical shift imaging grid (red; zero filled to 32 × 32) and the stimulated echo box (*large black rectangle*). (*A*) Four spectra were extracted (position marked by *small black squares* 0.19 cm^3 in size) from the full magnetic resonance spectroscopic imaging data set. (*Top left*) Extracted spectra from the tumor center with poor signal-to-noise ratio (SNR) and residual signal from *N*-acetylaspartate (NAA) only. The extracted spectrum from the right brain hemisphere shows normal-appearing metabolic ratios (*bottom left*). The extracted spectrum from the tumor border (*top right*) and the spectrum from the normal appearing white matter (NAWM) (*bottom right*) at a distance of 2 to 3 cm from the tumor show increased choline (Cho)/NAA ratios. Note the limited SNR in single small voxels not suitable for quantification. (*B*) Four anatomy matched voxels (AMVs) were manually selected: AMV of the tumor center (*top left*) with poor SNR and residual signals from NAA and creatine. The AMV spectrum selected from the right brain hemisphere shows normal-appearing metabolic ratios (*bottom left*, Cho/NAA = 0.28). The selected AMVs from the tumor border (*top right*, marked with red squares) and the AMV spectrum from the NAWM (*bottom right*) show increased Cho/NAA ratios (Cho/NAA = 0.48 and 0.58, respectively).

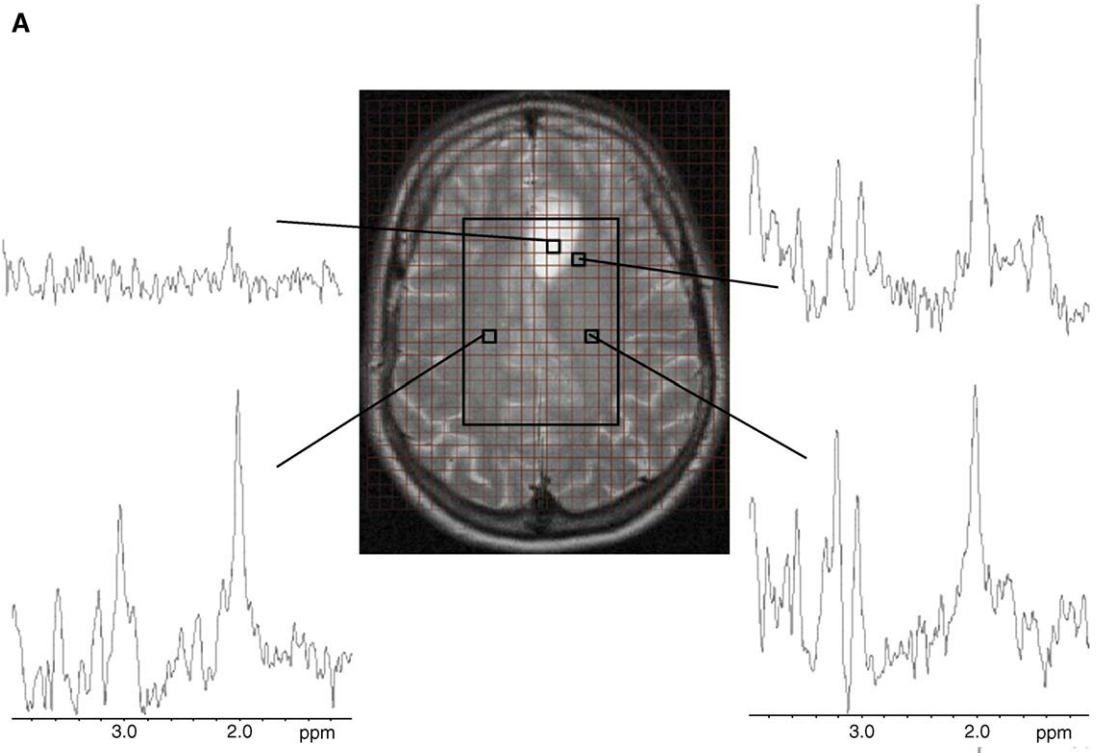
A
3.0
2.0
ppm
3.0
2.0
ppm

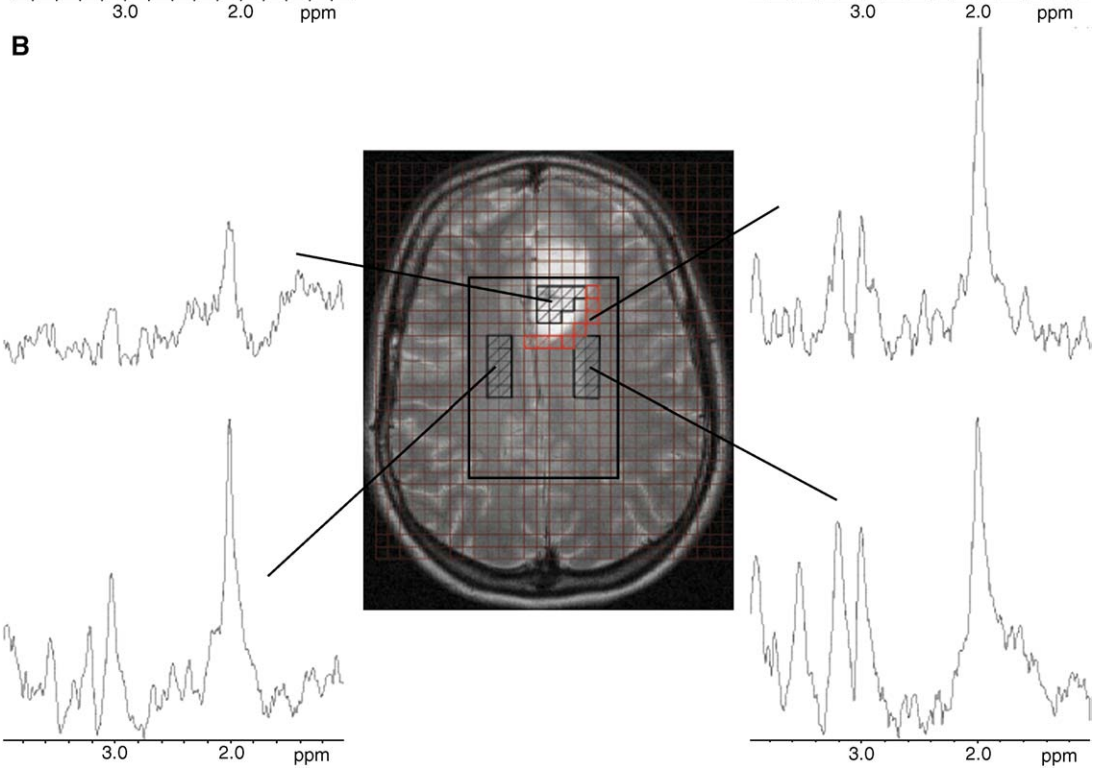
B
3.0
2.0
ppm
3.0
2.0
ppm

cedure [74], resulting in an approximately 9 Hz water line width for the whole PRESS or STEAM box.

Data processing at 3 T

Hadarmard transformation is performed in the z-direction (ie, along the magnet and patient axis), and a fast FT is performed in the other two spatial directions. This includes zero filling to 32 × 32 in the x-y plane, resulting in a minimum voxel size of 0.19 cm^3 (nominal voxel size was 0.33 cm^3 for healthy volunteers and 0.75 cm^3 for patients, respectively). Specific voxels forming an anatomically or pathologically matched AMV are chosen manually. Each spectrum is corrected for zero-order and first-order phase shifts and is aligned to the NAA or Cho signal. These spectra are summed, resulting in the AMV spectrum, which is then processed with CSX.

Results at 3 T and discussion of their potential value for clinical diagnosis

Long– and short–echo time high-resolution three-dimensional magnetic resonance spectroscopic imaging of human white matter

Fig. 4 shows two AMV spectra, both acquired with a nominal resolution of 0.33 cm^3. On the left side, a long TE (135 milliseconds) AMV spectrum summed up to 36 cm^3 is shown. The short TE (11 milliseconds) AMV spectrum was summed up to 31 cm^3. Both AMV spectra were obtained from healthy white matter approximately 1 cm caudal to the ventricles. The spectral resolution (note the separation between the Cho and Cr resonance) and SNR of both spectra are excellent compared with the single-voxel reference (see Fig. 1). This is the main advantage of high-resolution ^{1}H-MRSI. Anatomically or pathologically matched voxels can be defined after the measurement, minimizing partial volume contaminations. Because of the different T_2-relaxation times of Cr and Cho, the metabolic ratios of Cho/Cr are different for the two experiments. A quantitative comparison is only possible with data measured with the same TE at the same field strength.

Short–echo time three-dimensional magnetic resonance spectroscopic imaging

A female patient (31 years old) presented with a frontal hyperintense lesion after a horse-riding accident with the primary diagnosis of a possible glioma. Fig. 5A shows four voxels extracted from the left (containing the tumor) and right hemispheres marked on the high-resolution MRI scans. The extracted white matter spectrum from the contralateral side appears normal, whereas the spectrum extracted from the ipsilateral normal appearing white matter (NAWM) (the distance to the tumor border is approximately 2.5 cm) and the tumor border (red voxels) shows increased Cho and decreased NAA. Compared with an age- and sex-matched control subject, the Cho/NAA ratio was increased by 50% to 70%. Fig. 5B shows the same anatomic slice overlaid with the CSI grid and the STEAM box. Four AMV spectra resulting from 10 zero-filled voxels summed up to 1.9 cm^3 each are presented. Again, the AMV spectrum from the NAWM in the tumor-containing hemisphere and the AMV spectrum from the tumor border show an increased Cho/NAA ratio compared with spectra of an age- and sex-matched control and with the AMV spectrum of white matter taken from the contralateral side.

Because of the low concentration of the "NMR-visible" metabolites, the resolution achieved in most ^{1}H-MRS studies was in the centimeter range compared with the standard millimeter range in conventional MRI. Problems thus often result from partial volume effects.

The first whole-body 3 T scanners became available only a few years ago and allow an improvement in SNR by a factor of two compared with 1.5-T systems if other parameters are assumed to be constant. It has been shown, however, that the T_2-relaxation times of relevant metabolites are reduced at 3 T compared with 1.5 T, resulting in signal loss with the use of SE or stimulated echo techniques [75]. Nevertheless, in 3D MRSI with PRESS preselection (TE = 135 milliseconds), an improvement of approximately 23% to 46% could be achieved comparing 1.5 and 3 T [71]. Spectral dispersion also improves by a factor of 2 at 3 T, a gain partially eroded by broader line widths [71]. Recently, it has been demonstrated that a satisfactory SNR can be achieved using spatial resolutions less than 0.5 cm^3 at 3 T with a standard head coil [73] because of a nonlinear decrease in SNR with reduction of the voxel volume in the range of 0.5 to 0.1 cm^3. In a tumor patient, an AMV within an edema in the brain hemisphere contralateral to the MRI-visible tumor could be formed, without partial volume effects, because of the high voxel resolution of 0.33 cm^3 used [73]. Unexpectedly, the edema showed tumor-like metabolic patterns indicating tumor progression. The use of AMVs has the

potential to increase the diagnostic value of ^{1}H-MRSI as a result of higher specificity.

In addition, a 3D MRSI sequence with a TE of 11 milliseconds was developed in Vienna to compensate for signal losses caused by the shorter T_2-relaxation times at 3 T [76]. All spectra of the patient (0.75-cm^3 nominal resolution, acquisition time of 27 minutes) showed a satisfactory SNR, except for the spectra extracted from inside the tumor (see Fig. 5, top left). High spatial resolution, as shown in Fig. 4, also reduces susceptibility variations within a voxel, otherwise resulting in broadened and distorted spectral lines; thus, it may be useful to study "difficult" regions in the brain, such as the frontal lobe, temporal lobe, or brain stem [77]. The long acquisition time of approximately 1 hour currently limits the application of this technique to healthy subjects, however.

Outlook

High-field (ie, 3–5 T) in vivo MRI used within current legal limits for patient studies, combined with fast acquisition strategies [78] for time-consuming methods like 3D MRSI [79,80], should significantly improve diagnostic value (via SNR per unit time and spectral dispersion) and patient comfort (total measurement time) and, in addition, render the full combination of anatomic (CE-MRI), functional (blood oxygenation level dependent fMRI) [81], CE-susceptibility weighted imaging [82], perfusion [83], and metabolic imaging with sufficient spatial resolution possible for tumor patients. This combined information, if fully exploited for brain tumor diagnosis, staging, and therapy control, should have a significant impact on patient survival.

For brain research, ultrahigh-field MRI (7 T and higher) should have an impact on a better understanding of brain metabolism and physiology in healthy subjects. Because of increasing technical and methodologic problems (eg, homogeneity, specific absorption rate, shielding) as well as increasing costs, at least for a period of several years, these systems will be used for brain research only.

Acknowledgments

We are grateful to E. Knosp (Vienna, Austria) and R. Fahlbusch (Erlangen, Germany) for their expertise and generous support.

References

[1] Negendank W. Studies of human tumors by MRS: a review. NMR Biomed 1992;5(5):303–24.
[2] Ross B, Michaelis T. Clinical applications of magnetic resonance spectroscopy. Magn Reson Q 1994; 10(4):191–247.
[3] Falini A, Calabrese G, Origgi D, Lipari S, Triulzi F, Losa M, et al. Proton magnetic resonance spectroscopy and intracranial tumours: clinical perspectives. J Neurol 1996;243(10):706–14.
[4] Castillo M, Kwock L, Scatliff J, Mukherji SK. Proton MR spectroscopy in neoplastic and non-neoplastic brain disorders. Magn Reson Imaging Clin N Am 1998;6(1):1–20.
[5] Burtscher IM, Holtas S. Proton magnetic resonance spectroscopy in brain tumours: clinical applications. Neuroradiology 2001;43(5):345–52.
[6] Howe FA, Opstad KS. 1H MR spectroscopy of brain tumours and masses. NMR Biomed 2003; 16(3):123–31.
[7] Segebarth CM, Baleriaux DF, Luyten PR, den Hollander JA. Detection of metabolic heterogeneity of human intracranial tumors in vivo by 1H NMR spectroscopic imaging. Magn Reson Med 1990; 13(1):62–76.
[8] Paulus W, Peiffer J. Intratumoral histologic heterogeneity of gliomas. A quantitative study. Cancer 1989;64(2):442–7.
[9] Alesch F, Pappaterra J, Trattnig S, Koos WT. The role of stereotactic biopsy in radiosurgery. Acta Neurochir Suppl (Wien) 1995;63:20–4.
[10] Mihara F, Numaguchi Y, Rothman M, Sato S, Fiandaca MS. MR imaging of adult supratentorial astrocytomas: an attempt of semi-automatic grading. Radiat Med 1995;13(1):5–9.
[11] Bernstein M, Parrent AG. Complications of CT-guided stereotactic biopsy of intra-axial brain lesions. J Neurosurg 1994;81(2):165–8.
[12] Yu X, Liu Z, Tian Z, Li S, Huang H, Xiu B, et al. Stereotactic biopsy for intracranial space-occupying lesions: clinical analysis of 550 cases. Stereotact Funct Neurosurg 2000;75(2–3):103–8.
[13] Sawin PD, Hitchon PW, Follett KA, Torner JC. Computed imaging-assisted stereotactic brain biopsy: a risk analysis of 225 consecutive cases. Surg Neurol 1998;49(6):640–9.
[14] Field M, Witham TF, Flickinger JC, Kondziolka D, Lunsford LD. Comprehensive assessment of hemorrhage risks and outcomes after stereotactic brain biopsy. J Neurosurg 2001;94(4):545–51.
[15] Kreth FW, Muacevic A, Medele R, Bise K, Meyer T, Reulen HJ. The risk of haemorrhage after image guided stereotactic biopsy of intra-axial brain tumours—a prospective study. Acta Neurochir (Wien) 2001;143(6):539–545; discussion 545–6.
[16] Christy PS, Tervonen O, Scheithauer BW, Forbes GS. Use of a neural network and a multiple regression model to predict histologic grade of

astrocytoma from MRI appearances. Neuroradiology 1995;37(2):89–93.
[17] Klug N, Ellams ID. Advances in neurosurgery, vol. 9. Difficulties in the differential diagnosis of brain abscesses. Berlin: Springer-Verlag; 1981.
[18] Scully RE, Mark EJ, McNeely WF, Ebeling SH, Phillips LD. Case records of the Massachusetts General Hospital. Weekly clinicopathological exercises. Case 20–1997. A 74-year-old man with progressive cough, dyspnea, and pleural thickening. N Engl J Med 1997;336(26):1895–903.
[19] Arnold DL, Shoubridge EA, Villemure JG, Feindel W. Proton and phosphorus magnetic resonance spectroscopy of human astrocytomas in vivo. Preliminary observations on tumor grading. NMR Biomed 1990;3(4):184–9.
[20] de Graaf RA. In vivo NMR spectroscopy. New York: Wiley; 1998.
[21] de Certaines JD, Bovee W, Podo F. Magnetic resonance spectroscopy in biology and medicine. Tarrytown, NY: Pergamon Press; 1992.
[22] Smith JK, Castillo M, Kwock L. MR spectroscopy of brain tumors. Magn Reson Imaging Clin N Am 2003;11(3):415–29 [v–vi].
[23] Bruhn H, Michaelis T, Merboldt KD, Hanicke W, Gyngell ML, Hamburger C, et al. On the interpretation of proton NMR spectra from brain tumours in vivo and in vitro. NMR Biomed 1992;5(5):253–8.
[24] Howe F, Barton SJ, Cudlip SA, Stubbs M, Saunders DE, Murphy M, et al. Metabolic profiles of human brain tumors using quantitative in vivo 1H magnetic resonance spectroscopy. Magn Reson Med 2003;49:223–32.
[25] Provencher SW. Estimation of metabolite concentrations from localized in vivo proton NMR spectra. Magn Reson Med 1993;30(6):672–9.
[26] van der Veen JW, de Beer R, Luyten PR, van Ormondt D. Accurate quantification of in vivo 31P NMR signals using the variable projection method and prior knowledge. Magn Reson Med 1988;6(1): 92–8.
[27] Usenius JP, Tuohimetsa S, Vainio P, Ala-Korpela M, Hiltunen Y, Kauppinen RA. Automated classification of human brain tumours by neural network analysis using in vivo 1H magnetic resonance spectroscopic metabolite phenotypes. Neuroreport 1996;7(10):1597–600.
[28] Preul MC, Caramanos Z, Leblanc R, Villemure JG, Arnold DL. Using pattern analysis of in vivo proton MRSI data to improve the diagnosis and surgical management of patients with brain tumors. NMR Biomed 1998;11(4–5):192–200.
[29] Tate AR, Majos C, Moreno A, Howe FA, Griffiths JR, Arus C. Automated classification of short echo time in in vivo 1H brain tumor spectra: a multicenter study. Magn Reson Med 2003;49(1): 29–36.
[30] Kwock L, Smith JK, Castillo M, Ewend MG, Cush S, Hensing T, et al. Clinical applications of proton MR spectroscopy in oncology. Technol Cancer Res Treat 2002;1(1):17–28.
[31] Negendank WG, Sauter R, Brown TR, Evelhoch JL, Falini A, Gotsis ED, et al. Proton magnetic resonance spectroscopy in patients with glial tumors: a multicenter study. J Neurosurg 1996;84(3):449–58.
[32] Ricci PE, Pitt A, Keller PJ, Coons SW, Heiserman JE. Effect of voxel position on single-voxel MR spectroscopy findings. AJNR Am J Neuroradiol 2000;21(2):367–74.
[33] Gruber S, Frey R, Mlynarik V, Stadlbauer A, Heiden A, Kasper S, et al. Quantification of metabolic differences in the frontal brain of depressive patients and controls obtained by 1H-MRS at 3 tesla. Invest Radiol 2003;38(7):403–8.
[34] Haacke EM, Brown RW, Thompson MR, Venkatesan R. Magnetic resonance imaging: physical principles and sequence design. New York: Wiley; 1999.
[35] von Kienlin M. Empfindlichkeit und Ortsauflösung in der lokalisierten NMR-Spektroskopie. Universität Würzburg: Habilitationsschrift; 1996.
[36] McLean MA, Woermann FG, Barker GJ, Duncan JS. Quantitative analysis of short echo time (1)H-MRSI of cerebral gray and white matter. Magn Reson Med 2000;44(3):401–11.
[37] Nelson SJ, Vigneron DB, Star-Lack J, Kurhanewicz J. High spatial resolution and speed in MRSI. NMR Biomed 1997;10(8):411–22.
[38] Stadlbauer A, Moser E, Gruber S, Nimsky C, Fahlbusch R, Granslandt O. Integration of biochemical tumor images into frameless stereotaxy using a MRI/MRSI hybrid data set. J Neurosurg 2004; 101:287–94.
[39] Bottomley PA, Drayer BP, Smith LS. Chronic adult cerebral infarction studied by phosphorus NMR spectroscopy. Radiology 1986;160(3):763–6.
[40] Haase A. Localization of unaffected spins in NMR imaging and spectroscopy (LOCUS spectroscopy). Magn Reson Med 1986;3(6):963–9.
[41] Vikhoff-Baaz B, Starck G, Ljungberg M, Lagerstrand K, Forssell-Aronsson E, Ekholm S. Effects of k-space filtering and image interpolation on image fidelity in (1)H MRSI. Magn Reson Imaging 2001;19(9):1227–34.
[42] Jacobs MA, Horska A, van Zijl PC, Barker PB. Quantitative proton MR spectroscopic imaging of normal human cerebellum and brain stem. Magn Reson Med 2001;46(4):699–705.
[43] Stadlbauer A, Moser E, Gruber S, Buslei R, Nimsky C, Fahlbusch R, et al. Improved delineation of brain tumors: an automated method for segmentation based on pathologic changes of 1H-MRSI metabolites in gliomas. Neuroimage, in press.
[44] Stadlbauer A, Ganslandt O, Gruber S, Buslei R, Nimsky C, Fahlbusch R, et al. Improved preoperative diagnostics of brain tumors by quantification of 1H-MRSI metabolites. In: International Society of Magnetic Resonance in Medicine. Kyoto; 2004.

[45] Go KG, Kamman RL, Mooyaart EL, Heesters MA, Pruim J, Vaalburg W, et al. Localised proton spectroscopy and spectroscopic imaging in cerebral gliomas, with comparison to positron emission tomography. Neuroradiology 1995;37(3):198–206.
[46] Fulham MJ, Bizzi A, Dietz MJ, Shih HH, Raman R, Sobering GS, et al. Mapping of brain tumor metabolites with proton MR spectroscopic imaging: clinical relevance. Radiology 1992;185(3):675–86.
[47] Mader I, Roser W, Hagberg G, Schneider M, Sauter R, Seelig J, et al. Proton chemical shift imaging, metabolic maps, and single voxel spectroscopy of glial brain tumors. MAGMA 1996;4(2):139–50.
[48] Preul MC, Caramanos Z, Collins DL, Villemure JG, Leblanc R, Olivier A, et al. Accurate, noninvasive diagnosis of human brain tumors by using proton magnetic resonance spectroscopy. Nat Med 1996; 2(3):323–5.
[49] Kamada K, Saguer M, Moller M, Wicklow K, Katenhauser M, Kober H, et al. Functional and metabolic analysis of cerebral ischemia using magnetoencephalography and proton magnetic resonance spectroscopy. Ann Neurol 1997;42(4):554–63.
[50] Li X, Lu Y, Pirzkall A, McKnight T, Nelson SJ. Analysis of the spatial characteristics of metabolic abnormalities in newly diagnosed glioma patients. J Magn Reson Imaging 2002;16(3):229–37.
[51] De Edelenyi FS, Rubin C, Esteve F, Grand S, Decorps M, Lefournier V, et al. A new approach for analyzing proton magnetic resonance spectroscopic images of brain tumors: nosologic images. Nat Med 2000;6(11):1287–9.
[52] McKnight TR, Noworolski SM, Vigneron DB, Nelson SJ. An automated technique for the quantitative assessment of 3D-MRSI data from patients with glioma. J Magn Reson Imaging 2001;13(2): 167–77.
[53] Pirzkall A, McKnight TR, Graves EE, Carol MP, Sneed PK, Wara WW, et al. MR-spectroscopy guided target delineation for high-grade gliomas. Int J Radiat Oncol Biol Phys 2001;50(4):915–28.
[54] Pirzkall A, Nelson SJ, McKnight TR, Takahashi MM, Li X, Graves EE, et al. Metabolic imaging of low-grade gliomas with three-dimensional magnetic resonance spectroscopy. Int J Radiat Oncol Biol Phys 2002;53(5):1254–64.
[55] Nelson SJ, Graves E, Pirzkall A, Li X, Antiniw Chan A, Vigneron DB, et al. In vivo molecular imaging for planning radiation therapy of gliomas: an application of 1H MRSI. J Magn Reson Imaging 2002; 16(4):464–76.
[56] Ganslandt O, Steinmeier R, Kober H, Vieth J, Kassubek J, Romstock J, et al. Magnetic source imaging combined with image-guided frameless stereotaxy: a new method in surgery around the motor strip. Neurosurgery 1997;41(3):621–7; discussion 627–8.
[57] Ganslandt O, Fahlbusch R, Nimsky C, Kober H, Moller M, Steinmeier R, et al. Functional neuronavigation with magnetoencephalography: outcome in 50 patients with lesions around the motor cortex. J Neurosurg 1999;91(1):73–9.
[58] Jannin P, Fleig OJ, Seigneuret E, Grova C, Morandi X, Scarabin JM. A data fusion environment for multimodal and multi-informational neuronavigation. Comput Aided Surg 2000;5(1):1–10.
[59] Jannin P, Morandi X, Fleig OJ, Le Rumeur E, Toulouse P, Gibaud B, et al. Integration of sulcal and functional information for multimodal neuronavigation. J Neurosurg 2002;96(4):713–23.
[60] Nimsky C, Ganslandt O, Kober H, Moller M, Ulmer S, Tomandl B, et al. Integration of functional magnetic resonance imaging supported by magnetoencephalography in functional neuronavigation. Neurosurgery 1999;44(6):1249–55; discussion 1255–6.
[61] Sabbah P, Foehrenbach H, Dutertre G, Nioche C, DeDreuille O, Bellegou N, et al. Multimodal anatomic, functional, and metabolic brain imaging for tumor resection. Clin Imaging 2002;26(1):6–12.
[62] Croteau D, Scarpace L, Hearshen D, Gutierrez J, Fisher JL, Rock JP, et al. Correlation between magnetic resonance spectroscopy imaging and image-guided biopsies: semiquantitative and qualitative histopathological analyses of patients with untreated glioma. Neurosurgery 2001;49(4):823–9.
[63] Dowling C, Bollen AW, Noworolski SM, McDermott MW, Barbaro NM, Day MR, et al. Preoperative proton MR spectroscopic imaging of brain tumors: correlation with histopathologic analysis of resection specimens. AJNR Am J Neuroradiol 2001;22(4):604–12.
[64] Hall WA, Martin A, Liu H, Truwit CL. Improving diagnostic yield in brain biopsy: coupling spectroscopic targeting with real-time needle placement. J Magn Reson Imaging 2001;13(1):12–5.
[65] McKnight TR, von dem Bussche MH, Vigneron DB, Lu Y, Berger MS, McDermott MW, et al. Histopathological validation of a three-dimensional magnetic resonance spectroscopy index as a predictor of tumor presence. J Neurosurg 2002; 97(4):794–802.
[66] Rock JP, Hearshen D, Scarpace L, Croteau D, Gutierrez J, Fisher JL, et al. Correlations between magnetic resonance spectroscopy and image-guided histopathology, with special attention to radiation necrosis. Neurosurgery 2002;51(4):912–9; discussion 919–20.
[67] Preul MC, Leblanc R, Caramanos Z, Kasrai R, Narayanan S, Arnold DL. Magnetic resonance spectroscopy guided brain tumor resection: differentiation between recurrent glioma and radiation change in two diagnostically difficult cases. Can J Neurol Sci 1998;25(1):13–22.
[68] Roessler K, Nasel C, Czech T, Matula C, Lassmann H, Koos WT. Histological heterogeneity of neuroradiologically suspected adult low grade gliomas detected by Xenon enhanced computerized

tomography (CT). Acta Neurochir (Wien) 2003; 138(11):1341–7.

[69] Roessler K, Ungersboeck K, Czech T, Aichholzer M, Dietrich W, Goerzer H, et al. Contour-guided brain tumor surgery using a stereotactic navigating microscope. Stereotact Funct Neurosurg 1997;68(1–4 Part 1):33–8.

[70] Roessler K, Czech T, Dietrich W, Ungersboeck K, Nasel C, Hainfellner JA, et al. Frameless stereotactic-directed tissue sampling during surgery of suspected low-grade gliomas to avoid histological undergrading. Minim Invasive Neurosurg 1998; 41(4):183–6.

[71] Gonen O, Gruber S, Li BS, Mlynarik V, Moser E. Multivoxel 3D proton spectroscopy in the brain at 1.5 versus 3.0 T: signal-to-noise ratio and resolution comparison. AJNR Am J Neuroradiol 2001;22(9): 1727–31.

[72] Gruber S, Li BS, Soher BJ, Mlynarik V, Moser E, Gonen O. Head-to-head performance comparison of 3D multivoxel proton MR spectroscopy: 1.5 vs 3 tesla in the human brain. In: Radiologic Society of North America. Chicago; 2000.

[73] Gruber S, Mlynarik V, Moser E. High-resolution 3D proton spectroscopic imaging of the human brain at 3 T: SNR issues and application for anatomy-matched voxel sizes. Magn Reson Med 2003;49(2): 299–306.

[74] Gruetter R. Automatic, localized in vivo adjustment of all first- and second-order shim coils. Magn Reson Med 1993;29(6):804–11.

[75] Mlynarik V, Gruber S, Moser E. Proton T (1) and T (2) relaxation times of human brain metabolites at 3 tesla. NMR Biomed 2001;14(5):325–31.

[76] Mlynarik V, Gruber S, Stadlbauer A, Starcuk Z, Moser E. Anatomically matched short-echo time spectroscopy of human brain at 3T. In: European Society for Magnetic Resonance in Medicine and Biology, Rotterdam (NL), 2003, Nr. 390.

[77] Ebel A, Maudsley AA. Improved spectral quality for 3D MR spectroscopic imaging using a high spatial resolution acquisition strategy. Magn Reson Imaging 2003;21(2):113–20.

[78] Pruessmann KP, Weiger M, Scheidegger MB, Boesiger P. SENSE: sensitivity encoding for fast MRI. Magn Reson Med 1999;42(5): 952–62.

[79] Posse S, Tedeschi G, Risinger R, Ogg R, Le Bihan D. High speed 1H spectroscopic imaging in human brain by echo planar spatial-spectral encoding. Magn Reson Med 1995;33(1):34–40.

[80] Dydak U, Pruessmann KP, Weiger M, Tsao J, Meier D, Boesiger P. Parallel spectroscopic imaging with spin-echo trains. Magn Reson Med 2003;50(1): 196–200.

[81] Barth M, Nobauer-Huhmann IM, Reichenbach JR, Mlynarik V, Schoggl A, Matula C, et al. High-resolution three-dimensional contrast-enhanced blood oxygenation level-dependent magnetic resonance venography of brain tumors at 3 tesla: first clinical experience and comparison with 1.5 tesla. Invest Radiol 2003;38(7):409–14.

[82] Law M, Yang S, Wang H, Babb JS, Johnson G, Cha S, et al. Glioma grading: sensitivity, specificity, and predictive values of perfusion MR imaging and proton MR spectroscopic imaging compared with conventional MR imaging. AJNR Am J Neuroradiol 2003;24(10):1989–98.

[83] Ugurbil K, Adriany G, Andersen P, Chen W, Garwood M, Gruetter R, et al. Ultrahigh field magnetic resonance imaging and spectroscopy. Magn Reson Imaging 2003;21(10):1263–81.